

Joint Statistics of Strongly Correlated Neurons via Dimensional Reduction

Taşkın Deniz & Stefan Rotter

Bernstein Center Freiburg & Faculty of Biology,

University of Freiburg, Hansasträße 9a, 79104 Freiburg, Germany

(Dated: November 17, 2021)

Abstract

The relative timing of action potentials in neurons recorded from local cortical networks often shows a non-trivial dependence, which is then quantified by cross-correlation functions. Theoretical models emphasize that such spike train correlations are an inevitable consequence of two neurons being part of the same network and sharing some synaptic input. For non-linear neuron models, however, explicit correlation functions are difficult to compute analytically, and perturbative methods work only for weak shared input. In order to treat strong correlations, we suggest here an alternative non-perturbative method. Specifically, we study the case of two leaky integrate-and-fire neurons with strong shared input. Correlation functions derived from simulated spike trains fit our theoretical predictions very accurately. Using our method, we computed the non-linear correlation transfer as well as correlation functions that are asymmetric due to inhomogeneous intrinsic parameters or unequal input.

I. INTRODUCTION

Electric activity generated by different neurons in the brain is often strongly correlated [1–4]. These correlations arise as a result of shared input, or input components that are themselves correlated. Correlated activity can be a consequence of shared background fluctuations [5], but strong correlations might also indicate synchronous action potentials at the input indicating temporal coding. However, a clear-cut dichotomy between decorrelated and synchronized dynamics does not exist [6] [7, 8]. Rather, one should consider these two extremes as two faces of the same coin. Recent high-precision measurements reported very low average correlations suggesting a mechanism of active decorrelation in cortical networks [9–12]. At the same time it was observed by intracellular measurements that nearby neurons receive very similar input [2–4].

Several studies of pair correlations in neural networks relate structure and dynamics assuming a fluctuating dynamics about a fixed point that is characterized by asynchronous (A) population activity and irregular (I) spike trains [11, 13–15]. They employ essentially linear perturbation theory [16, 17] to compute correlation functions. Nevertheless, some of these works push the limits of existing methods. First of all, a qualitatively different AI state was observed in simulations of spiking neural networks with stronger couplings [18]. Secondly, a partial extension of the theory to the strongly correlated regime was based on numerically determined spike response functions [14]. Thirdly, pair correlation studies were generalized to higher-order correlations in recurrent networks by accounting for certain network connectivity motifs [19?]. These studies exploit and extend existing methods, but they also demonstrate the need for a new approach.

The main assumption of perturbation theory is that the common drive of the two neurons is weak. Yet, this criterion depends on the background state and strength of interactions in a given network. We showed previously that low background rates, for example, may lead to a breakdown of perturbation theory even for low correlation coefficients c [20]. This makes non-perturbative methods indispensable for modeling and analysis of correlations as low spike rates are typical in experiments [21]. All in all, a proper treatment of strong correlations must take the non-linear correlation transfer into account, which appears to play an important role in sensory processing [22]. However, a unified and transparent framework to calculate correlations of all strengths for neuron models of the integrate-and-fire type does

not exist.

The pitfall of previously suggested non-perturbative methods are their immense computational costs due to the high dimensionality of the discretized problem [23]. This makes computations practically impossible for a large range of parameters. For instance, the numerical effort of computing the pair correlation problem scales as N^4 , where N is the number of grid points used to approximate single neuron membrane potentials. Although, limiting the grid size is possible [24], a too coarse voltage grid fails to properly reflect the statistics of leaky-integrate-and-fire neurons with Poisson input. The precision issue gets even more severe for correlations of higher order, which are needed to parametrize the joint statistics of multiple neurons. With our methods, in contrast, we observed that joint membrane potential distributions of even strongly correlated neurons can be reduced to a small set of principal vectors via singular value decomposition (SVD). This suggests that strong correlations can be computed with high precision resorting to subspaces of relatively low dimension. In this work, specifically, we devise a SVD based method that allows to compute spike correlation functions of two leaky integrate-and-fire neurons with high accuracy.

Similar problems were studied analytically for arbitrary input correlations of the stochastic dynamics of neural oscillators [25], and for level-crossings of correlated Gaussian processes [26]. Related numerical work considered strong input correlations for integrate-and-fire neurons receiving white noise input [27] or shot noise input with nontrivial temporal correlations [28, 29]. The problem of analytically calculating the stationary distributions conditional on a spike from the exit current at the threshold is also discussed in the case of colored noise [28]. A method to deal with very strong input correlations ($c \approx 1$) in a specific input model (correlated Poisson processes) was suggested by [30]. Our study further suggests a novel technique, extending [24], to solve 2D jump equations for leaky integrate-and-fire neurons by mapping it to a Markov chain. This method provides an accurate estimate of the steady state joint distribution of membrane potentials.

We test our method for large input correlations c and demonstrate its power for different types of correlation asymmetries by comparing our semi-analytical approach to correlations extracted from simulated neuronal spike trains. We look at the full range of input correlations and provide an example of a non-linear correlation transfer function. Our method can be extended to more general integrate-and-fire models, higher-order input correlations and third order output correlations. However, we have to defer a detailed analysis of such cases

to future work.

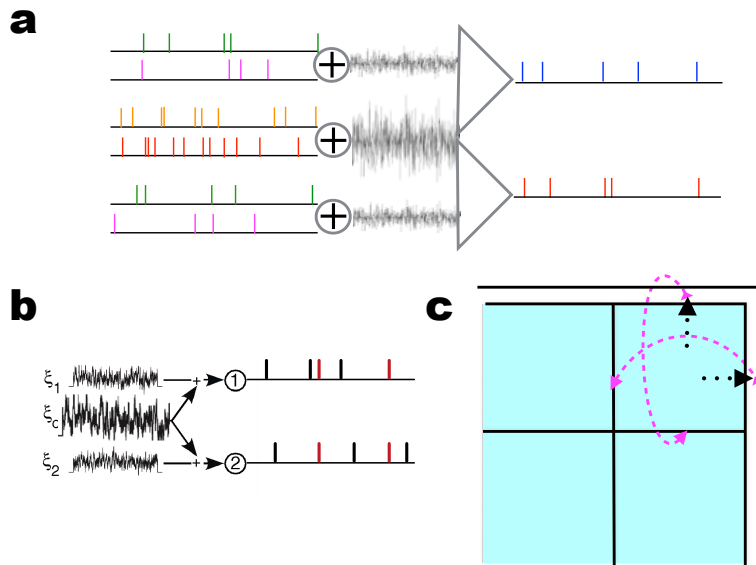


FIG. 1. (a) Two LIF neurons receiving private and shared shared inputs, both represented by excitatory and inhibitory spike trains. (b) Two neurons with shared white noise input, with first and second moments matched to (a). (c) Schematic describing the threshold crossing and reset mechanism that is part of the membrane potential dynamics of LIF neurons.

II. MODELS & METHODS

A. Two neurons with shared Poisson input

The leaky integrate-and-fire neuron model with postsynaptic potentials of finite amplitudes was studied previously in [24]. The stochastic equation that describes the membrane potential dynamics of one particular neuron is given as

$$\tau_m \dot{V}(t) = -V(t) + h_{ex}\tau \sum_i S_i^{ex}(t) + h_{in}\tau_m \sum_j S_j^{in}(t). \quad (1)$$

where h_{ex} and h_{in} represent the amplitudes of individual EPSPs and IPSPs, respectively, and $S_i^{ex}(t)$ and $S_j^{in}(t)$ are the spike trains of excitatory and inhibitory presynaptic neurons, with each of their spikes represented by a Dirac delta function

$$S_i^{ex}(t) = \sum_n \delta(t - t_n^i). \quad (2)$$

An analogous definition holds for inhibitory neurons. In both cases, if the membrane potential reaches the firing threshold, V_{th} , a spike is elicited and the voltage is reset to its resting value at 0.

In order to study correlations between the spike trains of two neurons we look at two coupled stochastic equations, describing the membrane potentials of two neurons that share a certain fraction of their excitatory and inhibitory input spikes

$$\dot{V}_1(t) = -\frac{V_1(t)}{\tau_{m,1}} + h_{ex}\left(\sum_k S_{1,k}^{ex}(t) + \sum_m S_m^{ex}(t)\right) + h_{in}\left(\sum_l S_{1,l}^{in}(t) + \sum_n S_n^{in}(t)\right) \quad (3)$$

$$\dot{V}_2(t) = -\frac{V_2(t)}{\tau_{m,2}} + h_{ex}\left(\sum_k S_{2,k}^{ex}(t) + \sum_m S_m^{ex}(t)\right) + h_{in}\left(\sum_l S_{2,l}^{in}(t) + \sum_n S_n^{in}(t)\right) \quad (4)$$

where shared excitatory and inhibitory input spike trains are denoted as $\sum_m S_{s,m}^{ex}(t)$ and $\sum_n S_{s,n}^{in}(t)$, respectively. Comparing the parameters of the jump model to shared white noise input we implicitly specified the firing rates of 6 independent Poisson processes (Fig. 1)

$$\dot{V}_1(t) = -\frac{V_1(t)}{\tau_{m,1}} + \mu_1 + \frac{\sigma_1}{\sqrt{\tau_{m,1}}}\xi_1(t) + \frac{\sigma_{c,1}}{\sqrt{\tau_{m,1}}}\xi_c(t) \quad (5)$$

$$\dot{V}_2(t) = -\frac{V_2(t)}{\tau_{m,2}} + \mu_2 + \frac{\sigma_2}{\sqrt{\tau_{m,2}}}\xi_2(t) + \frac{\sigma_{c,2}}{\sqrt{\tau_{m,2}}}\xi_c(t). \quad (6)$$

For notational convenience, shared input rates $r_{ex,c}$ and $r_{inh,c}$ are computed from a shared Wiener process ξ_c with zero mean. Setting $h_{ex} = h$ and $h_{in} = gh$, rates for each independent excitatory and inhibitory process are given as

$$r_{ex} = \frac{1}{1+g} \left(\frac{\sigma^2}{\tau h^2} + \frac{g\mu}{h\tau} \right) \quad (7)$$

$$r_{in} = \frac{1}{(g+g^2)} \left(\frac{\sigma^2}{\tau h^2} - \frac{\mu}{h\tau} \right). \quad (8)$$

Here we note that some combinations of (μ, σ) do not correspond to any combination of positive Poisson rates, as they must satisfy

$$\sigma^2 \geq h\mu \quad (9)$$

guarantee $r_{in} \geq 0$ for the inhibitory rate.

B. Discretized Markov operators for the LIF model

In this section we summarize the discrete approximation to the dynamics of a LIF neuron, as developed in [24]. The coarse graining of the membrane potential is given by the map

$$\mathbb{R} \rightarrow \mathbb{Z}, \quad V \mapsto \lfloor \frac{V}{\Delta V} \rfloor. \quad (10)$$

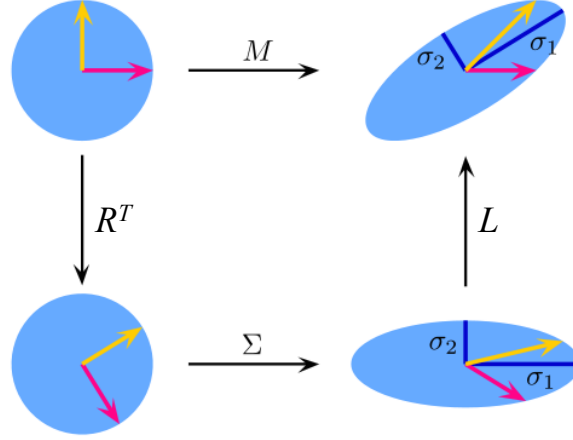


FIG. 2. Schematic illustration of Singular Value Decomposition in 2 dimensions, $M = L\Sigma R^T$, for positive definite matrices ($\det(M) > 0$). L and R are orthogonal matrices, and D is a real diagonal matrix. The non-negative diagonal elements σ_1 and σ_2 of the matrix Σ are the so-called singular values of the matrix M .

The probability density function $P(v)$ of the membrane potential then becomes a vector $p = (p_i)$ satisfying

$$p_i = \int_{v_i}^{v_{i+1}} P(v) dv, \quad (11)$$

with $v_i = i \Delta V$. As we impose a cut-off lower boundary V_- of the voltage scale, the dimension of the discrete state space is given as $N = \frac{V_{th} - V_-}{\Delta V}$.

The temporal evolution of the membrane potential distribution is now described in terms of a Markov process. The Markov propagator can be expressed as a juxtaposition of three operators: a decay operator \mathcal{D} describing leaky integration, a jump operator \mathcal{J} accounting for the action of synaptic inputs, and a threshold-and-reset operator \mathcal{T} that implements spike generation upon threshold crossing. The discrete decay operator \mathcal{D} is derived from its continuous counterpart D as follows

$$\begin{aligned} \Delta V \mathcal{D} \vec{p} &= \int_{v_i}^{v_{i+1}} DP(x) dx = \int_{v_i}^{v_{i+1}} \underbrace{e^{\Delta t / \tau_m}}_q P(e^{\Delta t / \tau_m} x) dx \\ &= \sum_{[q^i]}^{[q^{i+1}] - 1} p_j \cdot \Delta V + \left(\Delta V [q^i] - qv_i \right) p_{[q^i]} + \left(qv_{i+1} - \Delta V [q(i+1)] \right) p_{[q(i+1)]}. \end{aligned}$$

This definition leads to the following decay matrix

$$\mathcal{D}_{ij} = \sum_{k=\lfloor qi \rfloor}^{\lfloor q(i+1) \rfloor - 1} \delta_{j,k} + \left(\lfloor qi \rfloor - qv_i \right) \delta_{j, \lfloor qi \rfloor} + \left(qv_{i+1} - \lfloor q(i+1) \rfloor \right) \delta_{j, \lfloor q(i+1) \rfloor}. \quad (12)$$

The jump distribution, which underlies the jump operator \mathcal{J} , can be derived from the count distribution of excitatory and inhibitory synaptic events in a small time interval Δt . Assuming that they arrive with Poisson statistics (maximum entropy) at a rate of r_{ex} and r_{in} , respectively, we obtain

$$P(m, n) = \frac{a^m b^n}{m! n!} e^{-(a+b)} \quad (13)$$

where $a = r_{ex}\Delta t$ and $b = r_{in}\Delta t$ are the corresponding expected event counts. Dummy indices m and n correspond to excitatory and inhibitory counts. The jump distribution of the membrane potential $\gamma = (m - gn)h$ is given by

$$P(\gamma) = \sum_{m,n=0}^{\infty} P(m, n) \delta_{\gamma, (m-gn)h}. \quad (14)$$

The jump operator \mathcal{J} is then derived as

$$(\mathcal{J}p)_i = \sum_{\gamma} P(\gamma) p_{i - \frac{\gamma}{\Delta V}}$$

with a jump matrix given by

$$\mathcal{J}_{ij} = \sum_{\gamma} P(\gamma) \delta_{j, i - \frac{\gamma}{\Delta V}}. \quad (15)$$

The threshold-and-reset operator \mathcal{T} takes all the states above threshold and inserts them at the reset potential. This is simply given as

$$\mathcal{T}_{ij} = I_{j > \frac{v_{th}}{\Delta V}} \delta_{i, \frac{v_r}{\Delta V}} + I_{j \leq \frac{v_{th}}{\Delta V}} \delta_{i,j} \quad (16)$$

Finally, the time evolution matrix of the corresponding Markov chain is given as a product of the three operators described above

$$\mathcal{M} = \mathcal{T} \mathcal{J} \mathcal{D}. \quad (17)$$

The discrete stationary distribution is

$$\mathcal{M} P_0 = P_0, \quad (18)$$

and the corresponding stationary rate is given as

$$r_{\text{Markov}} = (\tau_{\text{ref}} + [\frac{1}{h} \sum_{i \geq i_{th}} (\mathcal{J} \mathcal{D} P_0)_i]^{-1})^{-1}. \quad (19)$$

C. Spike train correlations

The cross-covariance function of two stationary spike trains $S_a(t) = \sum_l \delta(t-t_l^a)$ ($a = 1, 2$) is defined as

$$C_{12}(\tau) = \langle S_1(t+\tau)S_2(t) \rangle - \langle S_1(t+\tau) \rangle \langle S_2(t) \rangle \quad (20)$$

where $\langle S_a(t) \rangle = r_a$, with $\langle \cdot \rangle$ indicating the ensemble average. For the model we studied here stationary rates were computed using Eq. 21. The cross-covariance function can be expressed in terms of the conditional firing rate $r_{1|2}(\tau)$, two stationary rates r_1 and r_2 , and the amplitude r_0 of a δ -function

$$C_{12}(\tau) = r_0\delta(\tau) + r_2(r_{1|2}(\tau) - r_1). \quad (21)$$

Given the spiking neuron model considered here, Eq. 21 can be derived from the stationary joint membrane potential distribution $P_0(V_1, V_2)$. Conditional on a spike at time t_0 in the first neuron, one has to find the instantaneous distribution of the membrane potential of the second neuron

$$P_{i|j}(V_i) = P(V_i | \text{neuron } j \text{ spikes at } t_0). \quad (22)$$

The probability of observing a consecutive spike is given by the flux $P_{\text{flux}}(V_1, \theta_2)$ with the normalization in Eq. 23. The conditional flux is computed for the Markov approximation as in Eq. 47. In general we simply compute the exit rate at the threshold distributed over V_1 by solving the following initial value problem

$$P(0, V_1) = P_{1|2}(V_1) = P_{\text{flux}}(V_1, \theta_2) \left(\int_{-\infty}^{\theta_1} P_{\text{flux}}(x, \theta_2) dx \right)^{-1} \quad (23)$$

$$\Delta_t P(t) = \mathcal{M}_1 P(t) \quad (24)$$

where \mathcal{M}_1 is discrete time evolution matrix of the neuron model given by Eq. 17. \mathcal{M}_1 leads to a (forward) time evolution in steps of Δt . The instantaneous conditional rate $r_{1|2}(t)$ in Eq. 21 is computed with a formula similar to Eq. 19

$$r_{1|2}(t) = r_{\text{Markov}}(t) = (\tau_{\text{ref}} + [\frac{1}{h} \sum_{i \geq i_{th}} (\mathcal{JDP}(t))_i]^{-1})^{-1}. \quad (25)$$

Finally, the covariance function $C_{21}(\tau)$ in Eq. 21 is derived by using $r_{1|2}(t)$ and two stationary rates r_1 and r_2 and r_0 . Note that the method described here can be generalized to higher order correlations as well.

D. Correlated jump distribution in 2D

We now use a 2-dimensional state space describing the joint membrane potential evolution of two neurons. Correlated and uncorrelated Poisson jumps push the 2D membrane potential vector (V_1, V_2) into three independent directions, $(1, 0)$, $(0, 1)$ and $(1, 1)$, allowing jumps in the positive (excitatory) and negative (inhibitory) direction, respectively. Hence, the jump distribution from an initial position (U_1, U_2) to a new position (V_1, V_2) in state space driven by 6 independent Poisson processes is obtained from a 2D convolution

$$P(V_1, V_2|U_1, U_2) = \int P_1(V_1 - U_1 - Z)P_2(V_2 - U_2 - Z)P_c(Z) dZ. \quad (26)$$

Inserting the expressions for the jump distributions in each direction, collecting all terms and using Eq. 13, we obtain

$$P(V_1, V_2) = \int \sum_{i,j=0}^{\infty} \sum_{k,l=0}^{\infty} \sum_{m,n=0}^{\infty} P_1(i, j) \\ \times P_2(k, l)P_c(m, n)\delta_{x-Z,(i-gj)h}\delta_{y-Z,(k-gl)h}\delta_{Z,(m-gn)h} dZ.$$

This expression is also valid for more general input statistic models that rely on a decomposition into statistically independent parts [30, 31]. Here we consider the shared Poisson input model as described by Eq. 4. Integrating the expression with respect to Z and inserting the mean event counts $a_i = r_{ex,i}\Delta t$ and $b_i = r_{in,i}\Delta t$, the resulting expression is given in a compact form

$$P(V_1, V_2) = \sum_{i,j=0}^{\infty} \sum_{k,l=0}^{\infty} \sum_{m,n=0}^{\infty} e^{-(a_1+b_1+a_2+b_2+a_s+b_s)} \\ \times \frac{a_1^i b_1^j}{i! j!} \frac{a_2^k b_2^l}{k! l!} \frac{a_s^m b_s^n}{m! n!} \delta_{V_1,(i-m-g(j-n))h} \delta_{V_2,(k-m-g(l-n))h}.$$

We can simplify this expression by choosing a regular grid according to $h_e = n\Delta V$ and $h_i = m\Delta V$, for integers m and n . In practice, however, the resulting sum will be truncated for a given tolerance. We will use the matrix form of the discretized operators in the following subsection, which is equivalent to the above expression.

E. Linear operators for correlated dynamics in 2D

Here we discuss the action of operators on state vectors of the discretized (V_1, V_2) space, assuming N bins in each dimension. We write the stationary voltage distribution in the

form

$$P_0(X, Y) \equiv \sum_{i,j=1}^N \Omega_{ij} X_i \otimes Y_j. \quad (27)$$

where X and Y are two suitable orthogonal bases of \mathbb{R}^N . We will define a specific choice for X and Y later in Section II F. As there is no crosstalk between the two neurons except by shared input leading to a correlated jump distribution, threshold and decay operators (tensors) are separable

$$\mathcal{D}_{2D} = \mathcal{D}_1 \otimes \mathcal{D}_2 \quad (28)$$

$$\mathcal{T}_{2D} = \mathcal{T}_1 \otimes \mathcal{T}_2. \quad (29)$$

Separability would also apply to the jump distribution for an input correlation coefficient of $c = 0$, corresponding to two neurons without shared input

$$\mathcal{J}_{2D} = \mathcal{J}_1 \otimes \mathcal{J}_2. \quad (30)$$

However, in the case of non-zero correlation, this relation holds only for a single path among the many connecting two points in state space. Therefore, every path must be taken into account by considering the contribution of each operator to a movement in the oblique (1, 1) direction.

Once we have computed the correct Markov matrix for 2D via

$$\mathcal{M}_{2D} = \mathcal{T}_{2D} \mathcal{J}_{2D} \mathcal{D}_{2D} \quad (31)$$

one can also find the stationary joint membrane potential distribution as the Perron-Frobenius eigenvector P_0 of the propagator matrix \mathcal{M}_{2D}

$$\mathcal{M}_{2D} P_0 = P_0. \quad (32)$$

Regarding the correlated jump distribution there are two ways of constructing \mathcal{J} operators. One possibility is described in Eq. 26. Alternatively, we construct linear Markov jump operators in 2D exploiting the commutativity of infinitesimal operators

$$\mathcal{J}_{2D} = e^{(J_1^p \otimes I + I \otimes J_2^p + J_1^c \otimes J_2^c)}.$$

Here I is the identity matrix. Using the properties of the operator product \otimes and commutativity of the individual factors, we can simplify this expression

$$\mathcal{J}_{2D} = (e^{J_1^p} \otimes I)(I \otimes e^{J_2^p})(e^{J_1^c \otimes J_2^c}).$$

In order to expand the third term we define U and D operators as up and down transition matrices, where U corresponds to a 1-step up transition, and D corresponds to a 1-step down transition. This leads to

$$U_{ij}^k = \delta_{i,j-k} \quad \text{and} \quad D_{ij}^l = \delta_{i,j+l}. \quad (33)$$

Hence, discrete approximations to infinitesimal generators of private components are given as

$$J_i = a_i U^k + b_i D^l. \quad (34)$$

where matrix powers k and l are defined on $h_e = k\Delta V$ and $h_i = l\Delta V$ for simplicity. (This restrictive assumption can be generalized easily by computing the continuous jump distribution in Eq. 14 and then discretizing it, which leads to the same result.) On the other hand, we need to be careful with correlated spikes, which trigger jumps into the oblique direction $(1, 1)$ with probability

$$c_{mn} = e^{-(a_c+b_c)} \frac{1}{m!} \frac{1}{n!} a_c^m b_c^n \quad (35)$$

for m excitatory and n inhibitory jumps. Expanding yields

$$\mathcal{J}_{2D} = \sum_{m=0} \sum_{n=0} c_{mn} [e^{J_1} U^{km} D^{ln} \otimes e^{J_2} U^{km} D^{ln}]. \quad (36)$$

As we noted before, the above construction is quite general and can be applied easily for general amplitude distributions. We only need to consider a discrete amplitude distribution c_{mn} in a given time bin of size Δt , as described above, see also [31, 32].

A final remark on the method described in this section concerns the commutativity of matrices. This property leads to a numerically more economic expression

$$\mathcal{J}_{2D} = \sum_{j \in \mathbb{J}} c(j) [e^{J_1} O^j \otimes e^{J_2} O^j] \quad (37)$$

where the set of integers \mathbb{J} is defined as list of all jump numbers $j = mk - nl$. The coefficient

$$c(j) = \sum_{m,n} e^{-(a_c+b_c)} c_{mn} \delta_{j,mk-nl} \quad (38)$$

is the probability of j jumps. The jump generator O is then defined in terms of matrix powers

$$O^j = \begin{cases} U^j, & j > 0 \\ I, & j = 0 \\ D^j & j < 0 \end{cases}. \quad (39)$$

F. Operator decomposition and SVD basis reduction

The expansion method described above is straightforward, but rather cumbersome to implement. We will now introduce a basis for the expansion of correlated jump operators suitable to reduce the cost of the computations involved, and helpful to increase the accuracy of a truncation. With our method, as compared to others, we have to solve linear equations of lower dimensionality in order to get a better approximation for the correlation function. Some further arguments for selecting Singular Value Decomposition are discussed in the results section. SVD of a matrix is given as

$$\mathcal{M} = \mathcal{L}\Sigma\mathcal{R}^T \quad (40)$$

where the diagonal entries of the diagonal matrix Σ are the square roots of the non-zero eigenvalues of $\mathcal{M}\mathcal{M}^T$ and $\mathcal{M}^T\mathcal{M}$. Both matrices \mathcal{R} and \mathcal{L} are orthogonal with columns consisting of the eigenvectors of $\mathcal{M}\mathcal{M}^T$ and $\mathcal{M}^T\mathcal{M}$, respectively. We show a 2D example SVD of Markov matrix in Fig. 2. For \mathcal{M} replaced by a single-neuron time evolution matrix \mathcal{M}_1 (\mathcal{M}_2), we define the matrix X (Y) by the selected orthogonal subspace of dimension K (L) of \mathcal{R}_1 (\mathcal{R}_2), according to the largest K (L) singular values, respectively. In order to project \mathcal{J}_1 (\mathcal{J}_2) and \mathcal{T}_1 (\mathcal{T}_2) to this subspace, we also extend the orthogonal basis X and Y to supra-threshold transitions

$$\tilde{X} = \begin{pmatrix} X & 0 \\ 0 & I_m \end{pmatrix}, \quad \tilde{Y} = \begin{pmatrix} Y & 0 \\ 0 & I_n \end{pmatrix}, \quad (41)$$

where X is an $M \times K$ and Y is an $N \times L$ operator, respectively. I_m and I_n are identity matrices, where m and n are the maximal supra-threshold jump numbers induced by both private and shared inputs. The combined action of \mathcal{J} and \mathcal{T} for $c = 0$ is then expressed as reduced operators

$$\mathcal{T}_1\mathcal{J}_1 \rightarrow X^T\mathcal{T}_1\tilde{X}\tilde{X}^T\mathcal{J}_1X, \quad \mathcal{T}_2\mathcal{J}_2 \rightarrow Y^T\mathcal{T}_2\tilde{Y}\tilde{Y}^T\mathcal{J}_2Y, \quad (42)$$

which map $M \times M$ ($N \times N$) to $K \times K$ ($L \times L$) matrices. Below we use the same dimensional reduction for correlated operators. In Eq. 37 the correlated jump operators are expressed as

$$\mathcal{J}_{2D} = \sum_{j \in \mathbb{J}} c(j) A_j \otimes B_j.$$

A dimensional reduction is then achieved by using Eq. 42 in

$$\mathcal{M}_{2D}P_0 = \sum_{j \in \mathbb{J}} c(j) (\mathcal{T}_1 A_j \mathcal{D}_1 \otimes \mathcal{T}_2 B_j \mathcal{D}_2) P_0.$$

In order to find P_0 in Eq. 27 we need to solve Eq. 32, which reads

$$\mathcal{M}_{2D}P_0 = P_0.$$

The projection operators $X^T \otimes Y^T$ satisfy $(X \otimes Y)(X^T \otimes Y^T)P_0 = P_0$. Applying them to the left hand side of this equation Eq. 32, we obtain

$$\begin{aligned} (X^T \otimes Y^T)\mathcal{M}_{2D} &= (X^T \otimes Y^T)\mathcal{M}_{2D}(X \otimes Y)(X^T \otimes Y^T)P_0 \\ &= \sum_{j \in \mathbb{J}} c(j) \left((X^T \mathcal{T}_1 \tilde{X} \tilde{X}^T A_j X X^T \mathcal{D}_1 X) \otimes (Y^T \mathcal{T}_2 \tilde{Y} \tilde{Y}^T B_j Y \mathcal{D}_2 Y) \right) \Omega \\ &\stackrel{RHS}{=} \Omega. \end{aligned}$$

$\Omega \equiv (X^T \otimes Y^T)P_0$ can be expressed in a simpler form as

$$\begin{aligned} (X^T \otimes Y^T)P_0 &= (X^T \otimes Y^T) \left(\sum_{ij} \Omega_{ij} X_i \otimes Y_j \right) \\ &= \sum_{ij} \Omega_{ij} X^T X_i \otimes Y^T Y_j \\ &= \sum_{ij} \Omega_{ij} e_i \otimes e_j \equiv \Omega \end{aligned}$$

for monomials $(e_i)_k = \delta_{i,k}$. The reduced equation is then

$$\mathcal{Q}\Omega = \Omega \tag{43}$$

where \mathcal{Q} is a tensor defined as

$$\mathcal{Q} = \sum_{j \in \mathbb{J}} c(j) (X^T \mathcal{T}_1 \tilde{X} \tilde{X}^T A_j X X^T \mathcal{D}_1 X) \otimes (Y^T \mathcal{T}_2 \tilde{Y} \tilde{Y}^T B_j Y \mathcal{D}_2 Y^T Y). \tag{44}$$

The dimensionally reduced problem in Eq. 43 can then be solved in practice by reindexing tensor indices $(i, j, k, l) \mapsto (I, K)$.

G. Conditional flux distribution

Using the decomposed 2D stationary distribution obtained by reduction, one can compute the flux distribution with the help of matrix operators. We compute the flux distribution

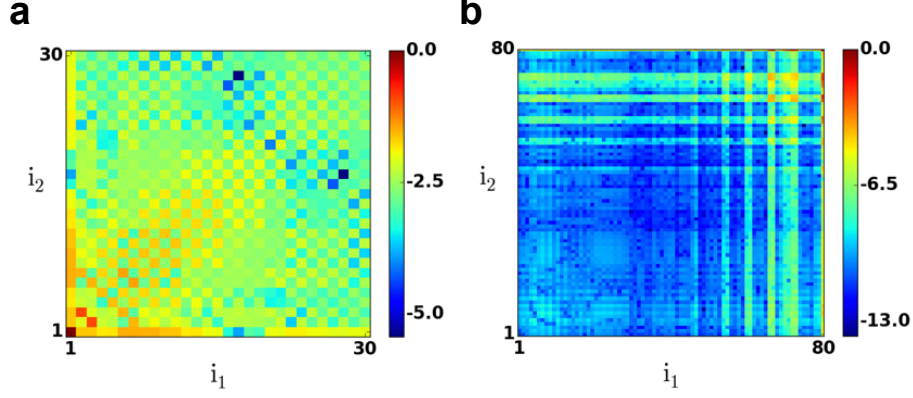


FIG. 3. Direct projections suffer from the imposed lower boundary and diverging dual eigenvectors. Therefore, we cannot increase the precision of our method using direct projections, as demonstrated above (a) we show components $\log_{10}(\Omega_{ij}/\max(S))$ with $N = 30$ eigenvectors via dual space projections. (b) Same as (a) with $N = 80$ eigenvectors. We observed that the example in (b) fails to converge as its maximum value is $S_{80,80}$, because of numerical instabilities.

using the 2D decay and jump operators with thresholding imposed only at one of the boundaries. A scheme illustrating the situation is shown in Fig. 1c. Here we explain how to obtain the flux distribution conditional on a spike in one neuron. In the general case of correlated neurons, the action of the full operators \mathcal{J}_{2D} and \mathcal{D}_{2D} is given as

$$\tilde{P}_{J,kl} = \mathcal{J}_{2D}\mathcal{D}_{2D}P_0 = \sum_{k',l'} \sum_{j \in \mathbb{J}} c(j)(A_j\mathcal{D}_1 \otimes B_j\mathcal{D}_2)_{kl,k'l'}(X_{k'}^T\Omega Y_{l'}), \quad (45)$$

where \tilde{P}_J is a $(M+m) \times (N+n)$ matrix. The implicitly summed subspace indices, $P_{0,kl} = \sum_{m,n} X_{k',m}^T\Omega_{mn}Y_{n,l'}$, are not shown and, A_j , B_j and $c(j)$ are defined in Eq. 37. This equation can be written in a concise form with implicit indices as

$$\tilde{P}_J = \sum_{j \in \mathbb{J}} c(j)A_j^T\mathcal{D}_1^T X^T\Omega Y\mathcal{D}_2 B_j = \tilde{X}^T\tilde{\Omega}\tilde{Y}.$$

Again, for practical reasons, computations were reduced by projecting $\mathcal{J}_{2D}\mathcal{D}_{2D}$ to extended subspaces \tilde{X} and \tilde{Y} similar to Eq. 42

$$\tilde{\Omega} = \sum_{j \in \mathbb{J}} c(j) \left[(\tilde{X}^T A_j X X^T \mathcal{D}_1 X) \otimes (\tilde{Y}^T B_j Y \mathcal{D}_2 Y) \right] \Omega. \quad (46)$$

In order to compute the probability of jumps we need to sum the probabilities for a jump over the threshold $V_1 > \theta_1$ or $V_2 > \theta_2$. The flux distribution is obtained as

$$P_{\text{flux},k} \propto \sum_{l=N}^{N+n} \tilde{P}_{J,kl} = \sum_{l=N}^{N+n} \tilde{X}_k^T \tilde{\Omega} \tilde{Y}_l, \quad P_{\text{flux},l} \propto \sum_{k=M}^{M+m} \tilde{P}_{J,kl} = \sum_{k=M}^{M+m} \tilde{X}_k^T \tilde{\Omega} \tilde{Y}_l \quad (47)$$

defined for $k < M$ and $l < N$. These expressions are normalized such that $\sum_k P_{\text{flux},k} = 1$. The amplitude of the delta singularity at the reset potential is obtained as

$$r_0 = r_{ex,c} \sum_{l=N}^{N+n} \sum_{k=M}^{M+m} \tilde{X}_k^T \tilde{\Omega} \tilde{Y}_l, \quad (48)$$

where $r_{ex,c}$ is the rate of excitatory shared spike trains. Once we have found the conditional flux distribution, we can solve the initial value problem defined in Eq. 23 in order to determine the conditional rates $r_{1|2}(t)$ or $r_{2|1}(t)$.

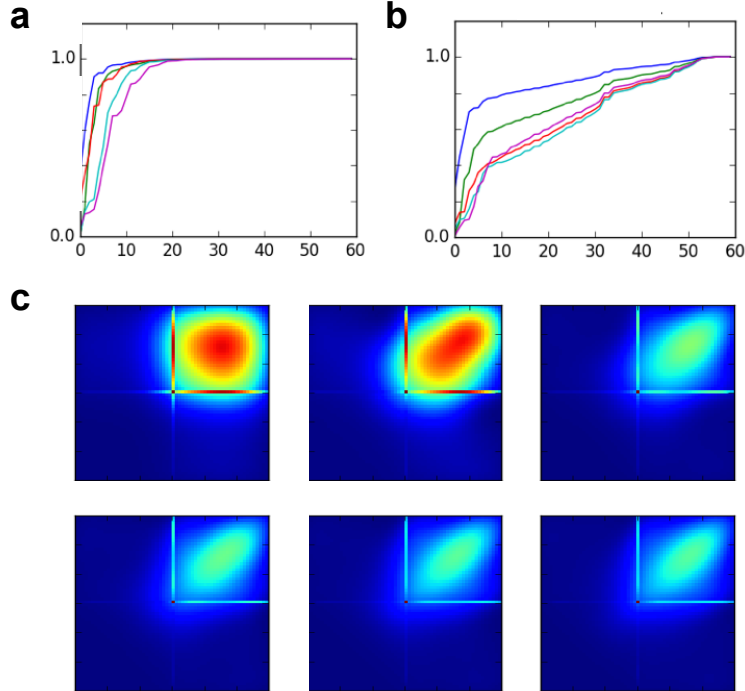


FIG. 4. Reverse engineering of a known stationary distribution. (a) Projections of a known stationary distribution (obtained by the full jump distribution as in 26) $P = \mathcal{L}\Sigma\mathcal{R}^T$ on the right singular vectors and (b) on the left singular vectors of the single-neuron time evolution matrix \mathcal{M} . The result is shown here for symmetric neuron parameters $\mathcal{L} = \mathcal{R} = W$. (c) Reconstruction of a stationary 2D joint membrane potential distribution. Singular vectors sorted by decreasing singular values and added one by one $P_{(K)} = \sum_{k=1}^K \sigma_k W_k \otimes W_k$, increasing the number of components from top left to bottom right. The convergence is relatively fast despite the rather high correlation of $c = 0.7$. Note that we used here a coarse grid $\Delta V = 0.5$ mV as the full solution (vs. the reduced solution we promote here) of the problem requires $O(N^4)$ operations.

H. Diffusion approximation vs. finite PSPs

We compare the exit rate of the stochastic system with post-synaptic potentials of finite amplitude with the analytic result obtained for the diffusion approximation [?]. For small enough PSPs the difference in rates of the two models is small

$$r_{sg}^{-1} = \tau_{\text{ref}} + \tau_m \sqrt{\pi} \int_{\frac{V_r - \mu}{\sigma}}^{\frac{V_{th} - \mu}{\sigma}} e^{x^2} [1 + \text{erf}(x)] dx \quad (49)$$

$$r_{\text{Markov}}^{-1} = \tau_{\text{ref}} + \left[\frac{1}{h} \sum_{i \geq i_{th}} (\mathcal{J}\mathcal{D}p)_i \right]^{-1} \quad (50)$$

We use the absolute difference between the two rates

$$r_{\text{error}}(\mu, \sigma) = |r_{sg}(\mu, \sigma) - r_{\text{Markov}}(\mu, \sigma)| \quad (51)$$

to account for the accuracy of a specific space-time grid $(\Delta V, \Delta t)$.

I. Correlation coefficient and comparison to diffusion approximation

The correlation coefficient in 10a is computed with the formula

$$C_{out}(c) = \frac{r_0 + \int r_2(r_{1|2}(\tau) - r_1) dt + \int r_1(r_{2|1}(\tau) - r_2) dt}{CV_1 CV_2 \sqrt{r_1 r_2}} dt. \quad (52)$$

We used 49 for the stationary rate r , r_0 is the amplitude of the δ -function in Eq. 48, and the coefficient of variation, $CV^2 = \frac{\sigma_{ISI}^2}{\mu_{ISI}^2}$, is computed with the equation

$$CV^2 = 2\pi r^2 \int_{\frac{V_r - \mu}{\sigma}}^{\frac{V_{th} - \mu}{\sigma}} e^{x^2} dx \int_{-\infty}^y [1 + \text{erf}(x)]^2 dy \quad (53)$$

as given in [13]. Thereby $\text{erf}(x)$ is the error function [33]. We computed correlation coefficients of the diffusion approximation of the finite PSP system (meaning a 2D Fokker-Planck equation with the same c and σ s) in [20].

J. Direct numerical simulations and data smoothing

We used the neural simulation tool NEST [34] to perform numerical simulations of input and output spike trains in the scenario described above. All analyses were based on discretized voltage data obtained during simulations of 1 000 s duration using a time resolution of $\Delta t = 10^{-4}$ s.

Empirical voltage distributions were obtained by normalizing histograms appropriately. Further smoothing using a simple moving average was performed before comparing these distributions to the analytically obtained stationary distribution. We also performed the comparison using cumulative distributions, as the implicit integration very efficiently reduces the noise in the data. Two 2D distributions are compared via visual inspection of contour lines. We also directly compare spike train cross-correlation functions to assess efficiency and accuracy of the method.

K. Numerical evaluation of cross-correlation functions

We compute cross-correlation functions of spike trains from conditional PSTHs. One can express this as an integral over two variables $\tau = t_1 - t_2$ and $s = t_1 + t_2$ with bin size Δ

$$C(\tau) = \frac{1}{\Delta} \int_{\tau}^{\tau+\Delta} \frac{d\tau'}{u(\tau') - l(\tau')} \int_{l(\tau')}^{u(\tau')} \sum_{i,j} \delta(\tau' - \tau_i) \delta(s' - s_j) ds' \quad (54)$$

where we set

$$u(\tau) = T/\sqrt{2} + |\tau|, \quad l(\tau) = T/\sqrt{2} - |\tau|. \quad (55)$$

with observation window T .

L. Convergence and error bounds

The direct singular value decomposition of a 2D membrane potential distribution shows that there are only few singular values that deviate significantly from 0 (Fig. 4). This behavior does not depend strongly on the chosen discretization, but it does depend on the input correlation coefficient c . Although singular vectors are not probability distributions in their own respect, the singular vectors X_i derived from the neuronal dynamics matrix (except the first few vectors) have the property

$$\sum_k X_{ik} \approx 0 \quad (56)$$

provided the discretization is fine enough. This behavior is demonstrated in Fig. 6. The contribution of each sum to the overall normalization

$$\sum_{ij} P_{ij} = \sum_{i,j} \sum_{k=0, l=0}^{K,L} X_{ik} \Omega_{kl} Y_{jl} = \Sigma_1 S \Sigma_2 \quad (57)$$

is progressively small, where Σ_{1k} and Σ_{2l} are sums of k -th and l -th singular vectors of the first and the second matrix for $k \geq m$ and $l \geq n$, respectively

$$\Sigma_{err}(m, n) = \sum_{i,j} \sum_{k=m, l=n}^{K,L} X_{ik} \Omega_{kl} Y_{jl} = \sum_{k=m, l=n}^{K,L} \Sigma_{1k} \Omega_{kl} \Sigma_{2l}. \quad (58)$$

This shows that the sum converges rather quickly. This error measure is related to projections of 1D discrete stationary distribution P_0 (satisfying $\mathcal{M}_1 P_0 = P_0$) to SVDs. All other eigenvectors of a Markovian matrix ($\mathcal{M}_1 P_0 = \lambda P_0$ for $|\lambda| < 1$) satisfy $\sum_k (P_i)_k = 0$. We want to avoid underestimating the total probability mass as a result of the truncated sum in Eq. 27. Hence, above we justify that the remainder of P_0 projections after truncation can be omitted up to a certain precision. On the other hand, in order to describe cumulative contribution of singular vectors we look at the L_1 distance of the omitted remainder (i.e. $k \geq m, l \geq n$)

$$E(m, n) = \sum_{i,j} |\Delta P_{ij}(m, n)| = \sum_{i,j} \left| \sum_{k=m, l=n}^{K,L} X_{ik} S_{kl} Y_{jl} \right| \quad (59)$$

which describes how well the method converges self-consistently. Here we didn't normalize this equation for every term we added. Which means we just rely on fast convergence of P_0 projections measured by Eq. 58, so first few error terms can be misleading.

III. RESULTS

In order to treat strong correlations we devised a robust numerical method to study the joint statistics of membrane potentials and spike trains of integrate-and-fire model neurons. The case study reported here covers the leaky integrate-and-fire (LIF) model with Poisson input spike trains. However, our method can be easily generalized to non-linear leak functions [35], conductance based synaptic inputs [36] and more complex input correlation models [30, 31],. although we have to leave the details of such generalizations open. In this section we will explain how to select a 'good basis for expansion', and we will give numerical examples that demonstrate the power of the method.

A. SVD of joint probability distributions and choice of expansion basis

We started from a simple observation: The stationary joint membrane potential distribution for two neurons with independent input is given as

$$P(V_1, V_2) = P_1(V_1)P_2(V_2) \quad (60)$$

where $P_1(V_1)$ and $P_2(V_2)$ are the stationary membrane potential distributions of two independent neurons, as described in Eq. 4. A similar relation for a discretized voltage grid can be written as

$$P = P_1 \otimes P_2. \quad (61)$$

For the case of shared input this simple relation is not valid any more. On the other hand, we observed that a value of the parameter c close to 0 will practically recruit only a small number of additional principal components for any given precision, cf. Fig. 4. Here we perform a singular value decomposition of the full solution of Eq. 32 given in terms of the matrix P_{ij}

$$P = \mathcal{L}\Sigma\mathcal{R}^T \quad \text{or} \quad P_{ij} = \sum_{k=1}^N \sigma_k L_{ik} R_{kj} \quad (62)$$

generalizing the case of independent neurons to also reconstruct the joint membrane potential distribution for neurons with shared input. As demonstrated in Fig. 4, convergence is rather quick, even for moderate values of c .

Another aim of our study was to gain some understanding about the influence of the space-time grid. We observed that left and right singular vectors are of the form

$$P_{kl} = \sum_{ij} \Omega_{ij} (X_{ik}^c + a_i \delta_{k,r}) (Y_{jl}^c + a_j \delta_{l,r}) \quad (63)$$

where X^c and Y^c reflect the quasi-continuous part of basis vectors and Ω is the coupling matrix as defined in Eq. 27. Here we need to make sure that the emerging singularity at the reset bin is not causing any numerical problems. One needs to first consider a small time step Δt and adapt the stepping in space Δx accordingly. A more thorough discussion of a suitable coarse graining strategy, however, is postponed to a later section of this paper.

Here we suggest to use SVD as a method to achieve a dimensional reduction of the full system. As it is a numerical method, its convergence and efficiency needs to be addressed. Generally, there are several different options to select a basis. Specifically, we use the

right singular vectors of single-neuron Markov matrices. As demonstrated in Fig. 4, right singular vectors lead to an expansion that converges faster for coarse grids (e.g. $V = 0.5$ mV). Although for finer grids (e.g. $V = 0.05$ mV) the difference is less prominent (Figs. 5a and b), right singular vectors still converge slightly faster than left singular vectors (Fig. 5d). Right singular vectors of the single-neuron time evolution matrix yield an orthogonal coordinate system with very good properties.

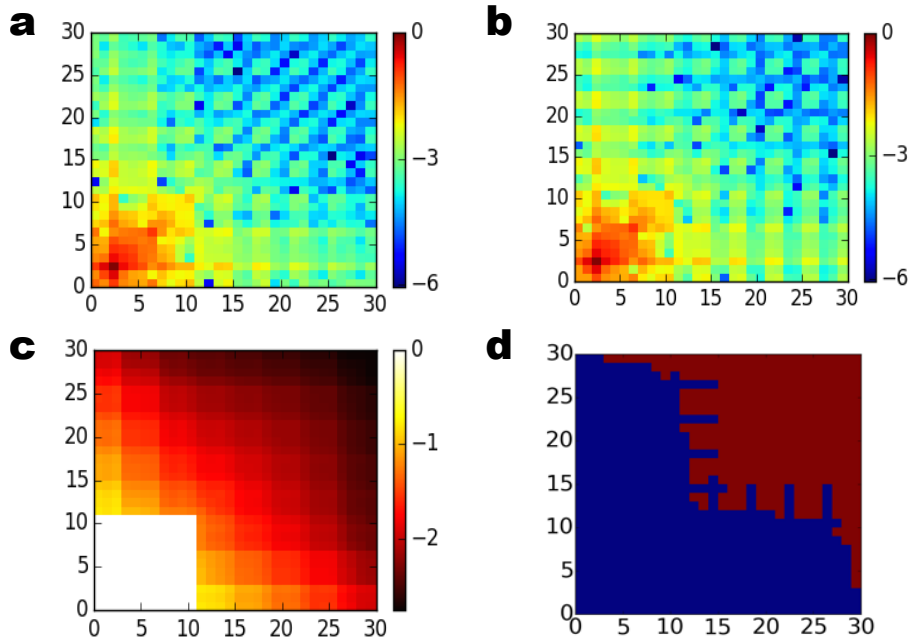


FIG. 5. Comparison of using right or left singular vectors for a reconstruction of the joint membrane potential distribution. We observe that the right singular vectors have better convergence properties. (a) Mode coupling matrix Ω for a basis derived from right singular vectors. (c) Partial sum error (Eq. 59) for the basis of right singular vectors, corresponding to (a). (b) Mode coupling matrix Ω for a basis derived from left singular vectors. (d) Difference of partial sum errors for left singular vectors corresponding to (b) and right singular vectors corresponding to (a). Red color indicates positive sign, while blue color indicates negative sign of the error. The reconstruction with right singular vectors converges slightly faster. Note that for the error measures considered in (c) and (d) we didn't take into account the bottom left 10×10 entries of the matrix.

As reported previously [20], we may also use a direct analytical approach using the basis

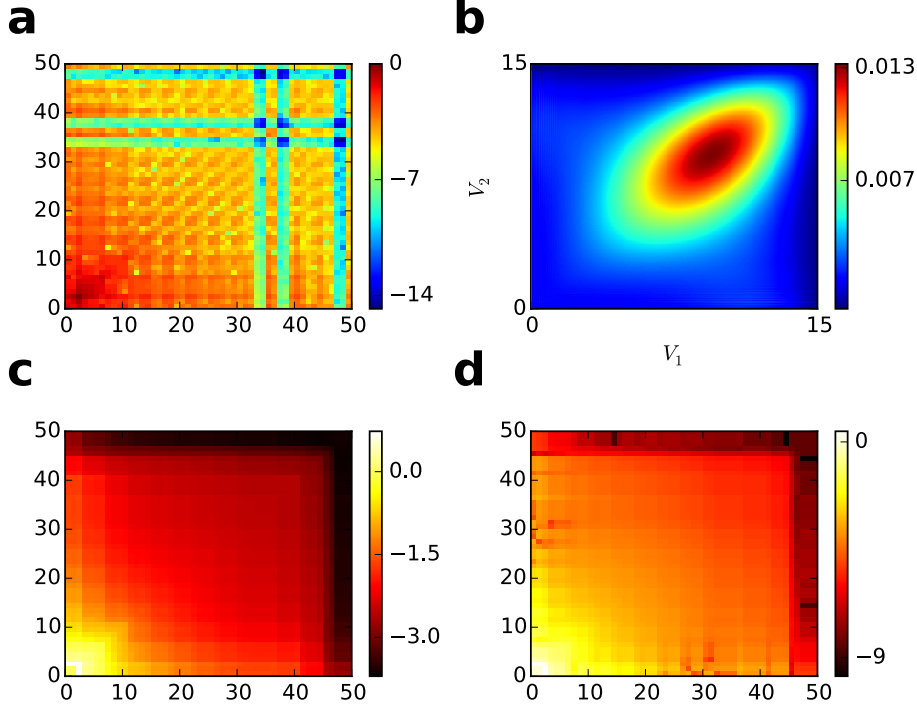


FIG. 6. Convergence of the SVD-based approximation method using up to 50 singular vectors corresponding to the largest singular values. (a) Mode coupling matrix Ω , defined by $P_0 = X^T \Omega Y$ (color represents $\log_{10}(\Omega_{ij}/\max_{ij}(\Omega_{ij}))$). (b) Reconstructed 2D membrane potential distribution based on a coarse graining with 50×50 grid points. (c) \log_{10} of relative L_1 error. The value given at location (i, j) is the contribution to the reconstruction of P computed via summation of all vectors $n > i, m > j$ (Eq. 59). (d) Error that arises from $\sum_k X_{ik} \neq 0$ (Eq. 58).

of the single-neuron Fokker-Planck operator, and its adjoint basis

$$P_0(X, Y) = \sum_{ij} \Omega_{ij} X_i \otimes Y_j \quad (64)$$

where X and Y are the left eigenvectors of the single neuron operators. However, the issue is that the discrete adjoint basis blows up at the lower boundary. The effect of this on our approximation is demonstrated in Fig. 3. In general, SVD eliminates a kernel of singular matrices.

In our treatment of the 2D Fokker-Planck equation, which is the infinitesimal limit of the theory considered above, we used the basis and adjoint basis to project linear operators to a subspace. This has certain advantages as it satisfies constraints for marginal distributions and preserves the Markov property to some extent. Positivity of the solution in the subspace

is not guaranteed, but time evolution is probability preserving ($\sum_i P_i(t) = 1$).

First, SVD is computationally convenient, because it leads to using a real orthogonal basis which resembles the eigenbasis of \mathcal{M} . Second, numerical instabilities due to an ill-conditioned time evolution matrix \mathcal{M} (some eigenvalues $\lambda_i \approx 0$) are cured by SVD. Third, although the basis vectors implied by SVD have the disadvantage of not completely preserving positivity, the deviation remains within tight bounds even for a relatively small number of basis vectors.

B. Comparison to direct numerical simulations

We compare our SVD-based Markov theory and direct numerical simulations of spiking neurons both on the level of joint 2D membrane potential distributions and on the level of spike train covariance functions, cf. Fig. 7. The empirical distributions derived from 2D histograms are slightly smoothed in order to compare them to the distributions derived from the Markov theory on the level of contour lines. We also considered 2D cumulative distribution functions, where the smoothing step can be omitted. Moreover, we computed output spike train covariance functions as described in methods section and compared them to the covariance functions obtained directly from the simulated spike trains.

C. Application 1: Non-linear correlation transfer

Two neurons that are driven by correlated input current will exhibit correlated output spike trains. This transfer of correlation reflects an important property of neuronal dynamics, which is of particular relevance for understanding the contribution of neurons to network dynamics. Recently, we were able to demonstrate, by exact analytical treatment, that the correlation transfer for leaky integrate-and-fire neurons is strongly non-linear [20]. Only for weak input correlation it can be described by perturbative methods, and deviations from linear response theory depend on the background firing rate. In the present work we demonstrate the same non-linear correlation transfer, cf. Fig. 10. There we also demonstrate how the parameters of the spatial and temporal coarse graining affects the precision of the Markov approximation. Our main conclusion is that dimensional reduction via SVD subspace projections makes it possible to achieve a superior precision with small bin sizes.

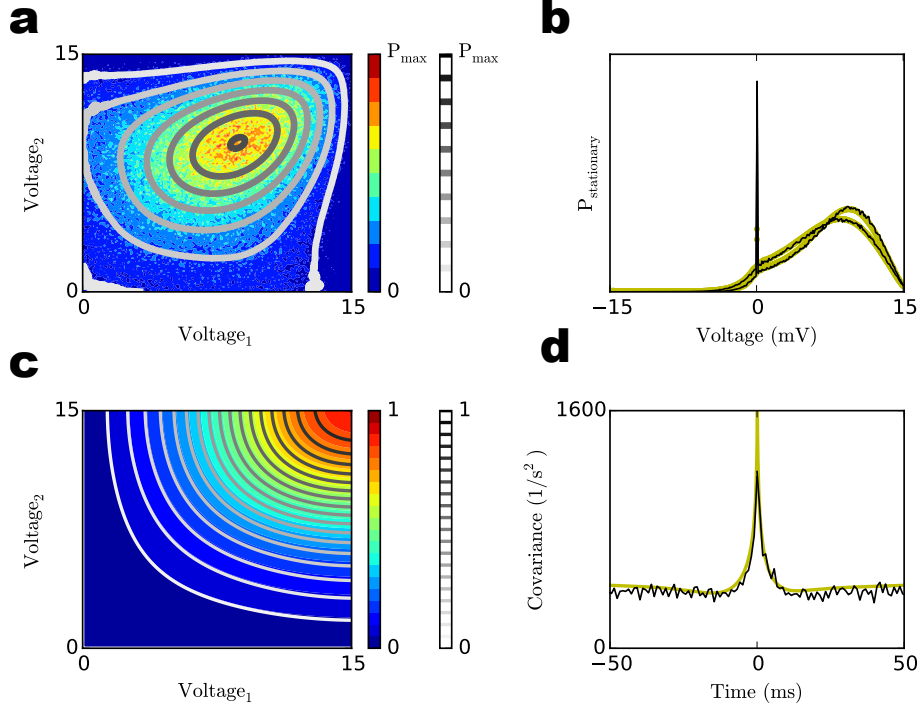


FIG. 7. Effect of different parameters of neurons or input to neurons (here, σ asymmetry) on the joint membrane potential distribution and spike cross-covariance function. Reconstruction of the 2D joint membrane potential distribution using SVD ($\Delta V = 0.1$ mV, $\Delta t = 0.1$ ms; grey contours) and comparison to direct numerical simulations (color-coded histograms). (a) Direct comparison of the SVD-based evaluation of the Markov theory and direct simulations. (b) Comparison of the corresponding 2D cumulative distributions. (c) Comparison of 1D marginal membrane potential distributions (yellow: Markov theory, black: direct simulation). (d) Comparison of spike train covariance derived from the Markov theory and direct simulations.

Fine enough grids, however, could not be dealt with on typical computers without using the reduction suggested here.

D. Application 2: Asymmetric cross-covariance functions

Neurons in biological networks have widely distributed parameters, and this heterogeneity may also influence information processing [38–40]. Moreover, robust asymmetries in spike correlations could lead to asymmetric synaptic efficacies, if they are subject to spike timing dependent plasticity [41, 42]. Our approach reveals a generic temporal asymmetry in cross-

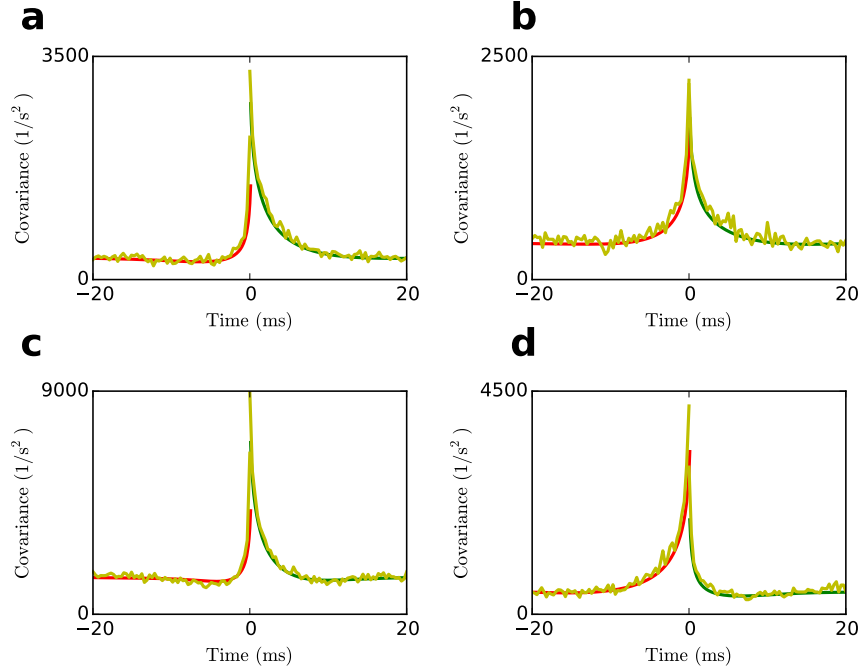


FIG. 8. Asymmetric cross-covariance functions in the strongly correlated regime ($c = 0.9$). Covariance functions extracted from simulated spike trains are compared to covariance functions computed with the SVD method suggested in this paper. Results are shown here for different types of asymmetry. (a) μ asymmetry, $\mu_1 \neq \mu_2$ while all other parameters are the same, (b) σ asymmetry, $\sigma_1 \neq \sigma_2$, (c) τ_m asymmetry, $\tau_1 \neq \tau_2$, which leads to $\mu_1 \neq \mu_2$ and $\sigma_1 \neq \sigma_2$ as private spike train input rates are the same, (d) V_{th} asymmetry, $V_{th,1} \neq V_{th,2}$. For specific parameter values, see Table II.

covariance functions, related to the heterogeneity of intrinsic neuron parameters and input variables. Such temporal asymmetry is more pronounced for larger values of c , especially in the non-perturbative regime that we address in this work.

We document here an application of our method to four types of asymmetries [20, 40]: μ asymmetry, σ asymmetry, τ_m asymmetry and V_{th} asymmetry. We quantified the asymmetry by $a = \chi_1/\chi_2$ (specific values given in Table II), where χ is replaced by the respective parameter. Asymmetric correlations have been described previously, and they were by numerical simulations and experimentally studied by [38, 40, 43, 44].

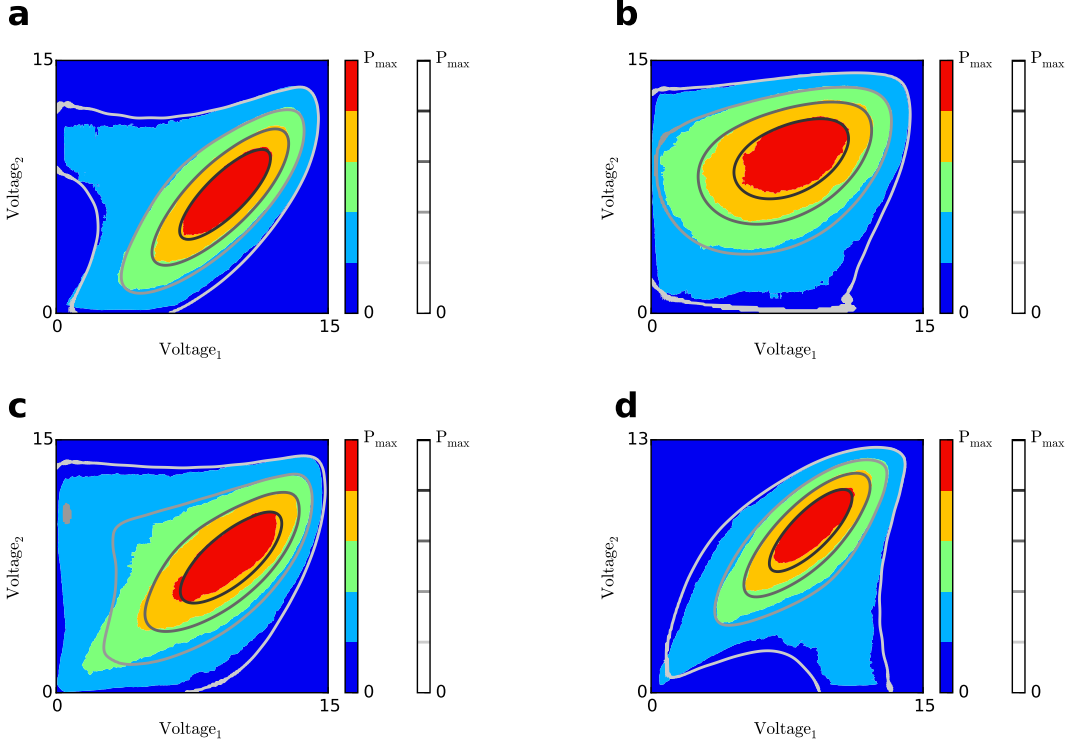


FIG. 9. Joint 2D membrane potential distribution of simulated neuron dynamics for $c = 0.9$ (2D histogram smoothed by boxcar kernel of width $w = 1$ mV) is compared to the joint distribution computed with the SVD method (using a subspace of dimension 50×50). We demonstrate here either heterogeneity in intrinsic parameters, or in input rate s . Both types of non-equal neuron parameters can lead to similar distributions. Our method can deal with all such cases accurately. Results are presented here for different asymmetric parameters: (a) μ asymmetry, (b) σ asymmetry, (c) τ_m asymmetry, which implies an asymmetry in μ and σ as well, as private spike train input rates are the same, (d) V_{th} asymmetry. For specific parameters, see Table II.

IV. DISCUSSION

A. Relevance of the new approach presented here

Models of correlated neuronal activity describe the origin of correlations in spiking model neurons, induced by the structure of the network and/or feedforward input. Such neuron models, however, are notoriously nonlinear. Nevertheless, most treatments rely on linearization and other simplifying assumptions, as nonlinear correlation transfer functions (i.e. rela-

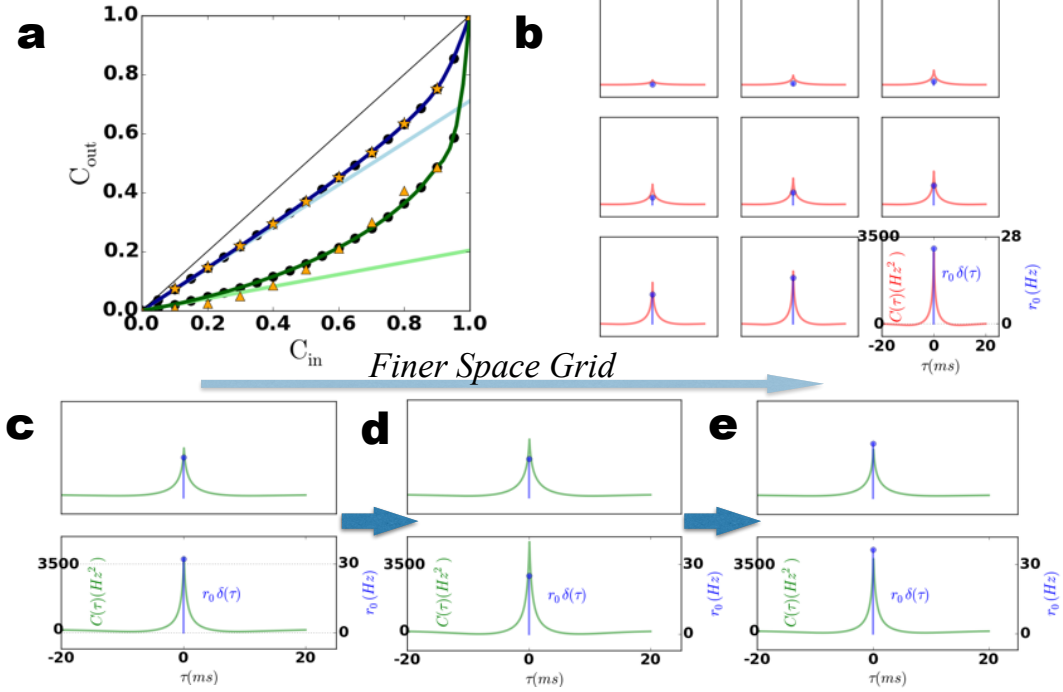


FIG. 10. Limits to the precision of cross-covariance functions and correlation transfer functions. (a) Correlation transfer function as a function of input correlation. We compare here analytical results (solid curves) described in a recent paper [20] with numerical results (orange symbols) obtained with the methods described in this paper. Non-perturbative correlation transfer functions $C_{out}(C_{in})$ in [20] for symmetric parameters and for high and low firing rates, respectively (blue: $r_b = 15.2 \text{ Hz}$, $CV^2 = 0.5$; green: $r_g = 1.13 \text{ Hz}$, $CV^2 = 0.98$). Slopes of light blue and light green lines (corresponding to $\frac{dC_{out}}{dC_{in}}$ at $C_{in} = 0$) are computed using perturbation theory [37]. Note that we added the obvious points $C_{out}(0) = 0$ and $C_{out}(1) = 1$ to the plot by hand. (b) Cross-covariance functions $C(\tau)$ (solid red curves, with unit H^2z^2) as a function of the lag τ . For non-infinitesimal PSPs there is a delta function at zero lag $\tau = 0$ (blue stems, with unit H^2z), the amplitude of which grows as c increases. Figures from top left to bottom right correspond to different values of c . For (a) and (b) we chose $\Delta V = 0.05 \text{ mV}$. Panels (c) and (d) are zoomed-in versions of the $c = 0.85$ (top) and $c = 0.95$ (bottom) covariance functions (solid green curves) to demonstrate the effect of the grid (c) $\Delta V = 0.05 \text{ mV}$ vs. (d) $\Delta V = 0.02 \text{ mV}$ vs. (e) $\Delta V = 0.01 \text{ mV}$. Further parameters are given in Table II

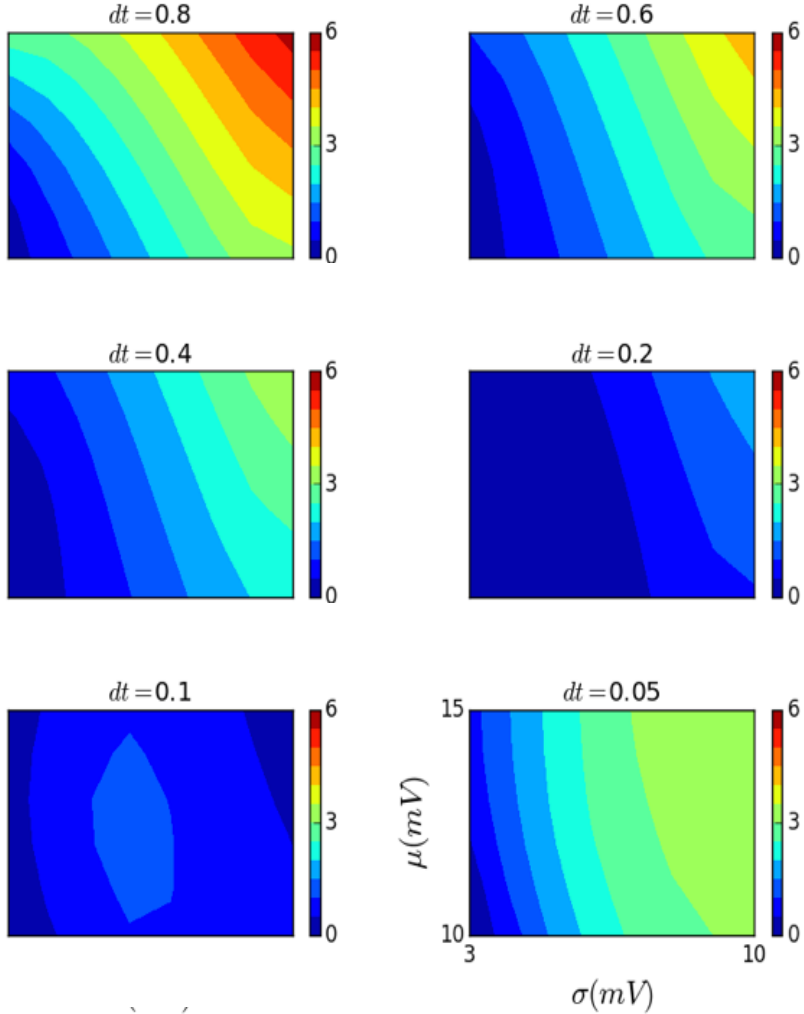


FIG. 11. Here we demonstrate that fixing the space bin (here $\Delta V = 0.02$ mV), the choice of the time bin affects the firing rate estimation [24]. The deviation of correlation coefficients for small rates in Fig. 10a (orange triangles vs. dark green curve) is a result of a poor estimation of conditional rates. The variance of the input (σ^2) is crucial in determining the appropriate temporal bin size, while the mean input (μ) is less effective. With increasing variance one observes an increasing firing rate error. From these plots, we conclude that for a space bin $\Delta V = 0.02$ mV, a time bin between $\Delta t = 0.2$ ms and $\Delta t = 0.1$ ms defines a range of good choices. All other parameters are as specified in Table I.

tion of input and output correlations) are difficult to derive. Previous analytical approaches have employed perturbation theory [16, 17] to study pairwise correlations under the assumption of weak input correlation [37, 45]. As a consequence of this technical convenience, we

still lack a systematic approach that allows us to deal with a broad range of correlations, and to gain an understanding of their implications for network dynamics.

B. Extensions of the theory

All computations described in our paper can be applied to more general integrate-and-fire models with a non-linear leak function $\Psi(V)$

$$\tau_m \dot{V} = \Psi(V) + J_{ex} \tau_m \sum_k S_k^{ex}(t) + J_{in} \tau_m \sum_k S_k^{in}(t). \quad (65)$$

We only need to rewrite the decay matrix as a discrete approximation of the differential operator $D(x) = \tau_m \frac{d}{dt} x - \Psi(x)$.

Other scenarios of interest are reflected by an altered amplitude distribution of the inputs. This is a natural consequence if individual synapses have different PSP amplitudes. It could also arise, however, if the population of input neurons has a non-trivial correlation structure. In particular, higher-order correlations have been treated in terms of specific amplitude distributions [31, 46]. The method described in the present paper can be adapted to such scenarios by simply using a modified definition of the jump matrix [30].

Higher-order statistics on the output side is also compatible with our method, describing the joint response behavior of three or more neurons that are driven by shared input. Third-order correlations can be computed in practice, because the projections work in the same fashion

$$P_{lmn} = \sum_{ijk} \Omega_{ijk} X_{il} Y_{jm} Z_{kn} \quad (66)$$

now with a 3D jump operator given in the generic form

$$J_{3D} = J_1 \otimes J_2 \otimes J_3. \quad (67)$$

This operator is again transformed with a basis derived from a SVD as

$$J_1 \otimes J_2 \otimes J_3 \rightarrow X J_x X^T \otimes Y J_y Y^T \otimes Z J_z Z^T. \quad (68)$$

This procedure is computationally more demanding as we need to consider additional paths, although the scaling is not exponential. Under assumption of homogeneous shared input

(same jump amplitudes driven by shared input in all directions) leads to an expression similar to Eq. 37,

$$\mathcal{J}_{3D} = \sum_{j \in \mathbb{J}} \psi(j) [e^{J_1 O^j} \otimes e^{J_2 O^j} \otimes e^{J_2 O^j}]. \quad (69)$$

Assuming joint stationarity of all three spike trains $S_1(t)$, $S_2(t)$ and $S_3(t)$, we need to find the joint third moment of the spike train statistics

$$\mu_{123}(\tau_1, \tau_2) = \langle S_1(\tau_1) S_2(\tau_2) S_3(0) \rangle. \quad (70)$$

As shown above, second moments can be computed with our method (Fig. 9). In order to obtain the covariance function from the stationary 3D flux, the time evolution of the 2D conditional flux at times (τ_1, τ_2) is needed. This is given as

$$\Delta_t P_{12|3}(t) = \mathcal{M}_{12} P_{12|3}(t) \quad (71)$$

which is computationally demanding as the numerical effort scales as $O(N^6)$. However, this can be projected to the subspace with time dependent coupling matrix Ω as

$$\Delta_t \Omega(t) = \mathcal{Q}_{12} \Omega(t). \quad (72)$$

This form has advantages over finite difference methods as e.g. suggested in [23]. The computation of the third order moment defined in Eq. 70 requires a solution of Eq. 72 at τ_2 to find the second conditional distribution $P_{1|2|3}(\tau_2)$. Then we need to find the 1D conditional distribution (e.g. for neuron 1) at $t = \tau_1$ by solving

$$\Delta_t P_{1|2|3}(t) = \mathcal{M}_1 P_{1|2|3}(t) \quad (73)$$

similar to Eq. 23. This provides us with conditional rate $r_{1|2|3}(\tau_1, \tau_2)$ and then the third moment is given as

$$\mu_{123}(\tau_1, \tau_2) = r_{1|2|3}(\tau_1, \tau_2) r_3. \quad (74)$$

Details of this computation have to be deferred to future work, though.

C. Boundary conditions and singularity

The joint membrane potential distribution has a singularity at the origin $(V_1, V_2) = (0, 0)$ due to a coordinated reset caused by some shared input spikes. There is also a line

discontinuity at $V_1 = 0$ and $V_2 = 0$, again due to the reset boundary condition. These singularities are reflected in the right singular vectors X and Y . This is the exact reason why we selected them as a basis to expand operators and joint distributions.

We observed that a singularity (a δ -function) emerges when ΔV is small and Δt is large, in relative terms. This is an issue even for the 1D discrete problem, and it is even more severe for 2D problems as the amplitude of the singularity scales quadratically with ΔV . This phenomenon occurs only if PSPs have a finite amplitude. As the PSP gets larger relative to ΔV , reset currents remain finite even in continuous time [24]. As a consequence, the limit to continuous variables must be taken with care, in particular for $c > 0$.

The δ -singularity does not exist for the diffusion approximation [20]. However, the definition of the current at the origin again fails as the derivative is discontinuous in both V_1 and V_2 directions. The infinitesimal limit of the jump equation must be taken with care. There is no doubt that the jump equation is well-defined as the flux at the boundary is not local. However, the infinitesimal limit is problematic for correlated neurons ($c > 0$) as the flux is not defined at the boundary of the 2D domain.

D. Precision, computational efficiency and grid selection

The selection of an appropriate grid in space and time is crucial for correlation computations. The small residual offset between direct simulation and our new semi-analytical computation (cf. Fig. 8 and 9), for example, can be considered as a discretization artifact. Although this issue would deserve a more systematic treatment, we report here some observations that can guide grid selection:

- (i) For discrete solutions of the heat equation based on central difference scheme, convergence of 1D time evolution requires $\frac{\Delta t}{(\Delta V)^2} < \frac{\tau}{\sigma^2}$ [47]. A similar rule also applies in the 2D case considered here. In general, explicit discretization schemes of second order differential operators arising in the study of diffusion, require positivity and stability conditions in the order of $\Delta t = O(\frac{\tau(\Delta V_1 + \Delta V_2)^2}{\sigma^2})$ [23]. In this work, we followed a discretization scheme that approximately conserves probability, a Markovian approximation [24]. However, we note once more that some grids may lead to violation of the Markov property for too large Δt , as a result of boundary effects. This may create issues when the largest eigenvalue exceeds 1.

- (ii) To reflect small expected bin counts (especially for $c \approx 1$) adequately, one needs a larger Δt and a smaller ΔV . This is in conflict with rule (i). Besides, we observe that smaller ΔV for a fixed Δt actually leads to better firing rate approximation up to some point (Fig. 11).
- (iii) A finer grid requires more computational efforts to achieve a smooth correlation function. The SVD reduction does not alter this behavior. Other dependencies and limiting factors are indicated in Fig. 10. There are two constraining factors which are determined by the selected precision of the approximation. One is the extent of the jump distribution, which affects the number of terms to be accumulated (size of the set \mathbb{J} in Eq. 37). For a fixed grid and a selected precision, this number increases with σ_c . The second constraint is the size of the SVD subspace. We know that as c gets closer to 1 and $C(\tau)$ gets steeper we need to include more singular components.

In Fig. 10 we illustrate how coarse graining affects the shape of the cross-covariance function $C(\tau)$. Although the precision of the approximation is limited by the subspace projections implied by SVD, the grid parameters Δt and ΔV are the most important factors to get the shape of the function right. However, for a fixed dimension of the SVD subspace even the finest grid would not be able to capture the singularity at zero time lag ($\tau = 0$). The grid effectively limits the precision of the approximation due to the reduced number of degrees of freedom.

V. CONCLUSION

We developed a novel numerical method to compute the joint statistics and correlation functions for two LIF model neurons driven by shared input. Our approach can deal with the full range of input correlations c , and the expansion converges fast. Also, our method is widely generalizable and can deal with other scenarios that are biologically relevant. We observed in previous work [20] that low output firing rates generally require a non-perturbative treatment. If output rates are high, in contrast, and for high input firing rates with small PSPs (diffusion regime), the approximation derived from linear response theory [37] is reasonably precise.

We conclude that it is possible to compute correlation functions (in contrast to deriving

them from simulations) for a wide range of models with finite PSP amplitudes, and also for a wide range of parallel spike train input models. Although there is currently no conclusive theory for the selection of an appropriate spatio-temporal grid, we were able to come up with some heuristics. The precision of even the first moment (firing rate) depends on the grid. Specifically if c is close to 1, the temporal component of the correlation function resembles a delta function. In order to capture this phenomenon the grid must be fine enough.

The innovation in our work is not only the formulation of correlation functions based on a Markov chain approximation, but also a dimensional reduction. This helps us compute joint membrane potential distributions. We showed that the number of components obtained by SVD needed to represent single neuron dynamical evolution matrices is small. This also means that computations can presumably be generalized to higher-order correlations with only moderately increased computational effort.

Systematic benchmarking of our method has not yet been performed. However, we believe our method constitutes the only reasonable numerical approximation to the joint statistics of strongly correlated neuronal dynamics with finite PSPs, apart from direct stochastic simulations [32]. This approximation for reasonable grids in space and time was only viable with SVD subspace projections.

APPENDIX: PARAMETERS

Table 1. Parameters for NEST simulations and semi-analytical computations

Neuron parameters: (Fig. 3, Fig. 5, Fig. 6, Fig. 7)		
Symbol	Description	Value
V_{th}	voltage threshold	15 mV
V_r	voltage reset	0 mV
τ_m	membrane time constant	15 ms
τ_{ref}	refractory period	1 ms
h	PSP	0.01 mV -0.1 mV
Δt	time resolution	0.1 ms
Input parameters		
μ	mean input	10-15 mV
σ_1, σ_2	STD private input	2-10 mV
σ_c	STD shared input	2-10 mV
c	input noise correlations	0-1
a	asymmetry factor	> 0

Table 2. Numerical results vs. NEST simulations : (Fig. 8, Fig. 9, Fig. 10)

Correlation asymmetry parameters		
Symbol	Description	Value
V_{th}	voltage threshold	15 mV
V_r	voltage reset	0 mV
τ_m	membrane time constant	15 ms
τ_{ref}	refractory period	1 ms
h	PSP	0.1 mV
μ	mean input	12. mV
σ_0	STD total input	5. mV for (b) and (d) , 6. mV for (a) and (c)
c	input noise correlations	0.9
a_σ	asymmetry factor	$1/\sqrt{2}$
a_μ	asymmetry factor	10/13
a_τ	asymmetry factor	10/15
$a_{V_{th}}$	asymmetry factor	13/15

*** asymmetry factors: $a = \chi_1/\chi_2$.

Table 3 Neuron model parameters

Symbol	Description	Unit
S^{ex}, S^{in}	spike trains	1/ms
V	membrane potential	mV
V_{th}	voltage threshold	mV
V_r	voltage reset	mV
t	time	ms
$\tau_{m,1}, \tau_{m,2}$	membrane time constant	ms
τ_{ref}	refractory period	ms
$h_{ex} = h, h_{in} = gh$	PSP	mV
μ	mean input	mV
σ_1, σ_2	STD private input	mV
σ_c	STD shared input	mV
σ_0	STD total input	mV
c	input noise correlations	0-1
r_e, r_i	ex & inh input rates	Hz
r_1, r_2	output rates of 2 neruons	Hz

Table 4 Correlations and related notation

Symbol	Description	Unit
$C(\tau)$	covariance function	Hz ²
$r_{1 2}(\tau)$	conditional rate	Hz
$P(V)$	probability distribution of V	1/mV
$P_{1 2}(V_1)$	conditional probability distribution of V_1	1/mV
$P(V_1, V_2)$	joint probability distribution of (V_1, V_2)	1/mV ²
Δ_t	discrete time evolution operator	1
\mathcal{M}_1	discrete time evolution matrix	1

Table 5 Probability distributions and Markov approximation

Symbol	Description	Unit
$P(q, r)$	probability for q excitatory, r inhibitory spike	1
$P(\gamma)$	probability for jumps of length γ	1
$P(V_1, V_2 V_{1,0}, V_{2,0})$	probability for jumps from $(V_{1,0}, V_{2,0})$ to (V_1, V_2)	1
$P(V_1, V_2)$	probability for jumps from $(0, 0)$ to (V_1, V_2)	1
\mathcal{T}	threshold matrix : $N \times (N + n)$	1
\mathcal{J}	jump matrix : $(N + n) \times N$	1
\mathcal{D}	decay matrix: $N \times N$	1
\mathcal{M}	time evolution matrix : $N \times N$	1
\mathcal{T}_{2D}	threshold tensor : $N \times M \times (N + n) \times (M + m)$	1
\mathcal{J}_{2D}	jump tensor : $(N + n) \times (M + m) \times N \times M$	1
\mathcal{D}_{2D}	decay tensor: $N \times M \times N \times M$	1
\mathcal{M}_{2D}	Time evolution tensor 2D : $N \times M \times N \times M$	1
U, D	up or down operators in discrete space	1
J_1^p, J_2^p	private V_1 or V_2 jump generators	1
J_1^c, J_2^c	shared V_1 or V_2 jump generators	1
c_{mn}	coefficient of m excitatory and n inhibitory jumps	1
P_0	stationary probability density in discrete space	$(\text{mV})^{-2}$
$P_{J,k}$	probability for jumps k -th component of $\mathcal{J}P_0$	1/mV
$P_{flux,k}$	probability for jumps k -th component conditional exit flux	1/mV
Δt	time bin	ms
ΔV	voltage bin	mV
a_1, b_1	average count of private input 1 in Δt	1
a_2, b_2	average count of private input 2 in Δt	1
a_c, b_c	average count of shared input in Δt	1

Table 6 SVD reduction

Symbol	Description	Unit
\mathcal{L}, \mathcal{R}	SVD left and right basis	1
Σ	singular value matrix	1
X, Y	SVD subspaces	1
\tilde{X}, \tilde{Y}	extended subspace	1
\mathcal{Q}	reduced operators defined on a selected subspace	1
M or N	size of full grid i.e. matrix	1
m or n	maximum number of jumps over the threshold	1
K or L	size of SVD subspace	1
$M + m$ or $N + n$	size of full jump subspace	1
$K + m$ or $L + n$	size of reduced jump subspace	1

Table 7 Asymmetry parameters

Symbol	Description	Unit
a_σ	asymmetry factor σ_1/σ_2	1
a_μ	asymmetry factor μ_1/μ_2	1
a_τ	asymmetry factor τ_1/τ_2	1
$a_{V_{th}}$	asymmetry factor $V_{th,1}/V_{th,2}$	1

-
- [1] R. Rosenbaum, T. Tchumatchenko, and R. A. Moreno-Bote, *Frontiers in Computational Neuroscience*, Vol. 8 (2014).
- [2] I. Lampl, I. Reichova, and D. Ferster, *Neuron* **22**, 361 (1999).
- [3] M. Okun and I. Lampl, *Nature Neuroscience* **11**, 535 (2008).
- [4] J. F. Poulet and C. C. Petersen, *Nature* **454**, 881 (2008).
- [5] A. Arieli, A. Sterkin, A. Grinvald, and A. Aertsen, *Science (New York, N.Y.)* **273**, 1868 (1996), arXiv:arXiv:1011.1669v3.
- [6] B. Staude, S. Rotter, and S. Grün, *Neural Computation* **20**, 1973 (2008).
- [7] A. Kumar, S. Rotter, and A. Aertsen, *Nat Rev Neurosci* **11**, 615 (2010).
- [8] B. Doiron, A. Litwin-Kumar, R. Rosenbaum, G. K. Ocker, and K. Josić, *Nature Neuroscience*

- 19**, 383 (2016).
- [9] A. S. Ecker, P. Berens, G. a. Keliris, M. Bethge, N. K. Logothetis, and A. S. Tolias, *Science* (New York, N.Y.) **327**, 584 (2010).
- [10] A. Renart, J. D. Rocha, P. Bartho, L. Hollender, N. Parga, A. Reyes, and K. D. Harris, **327**, 587 (2010).
- [11] V. Pernice, B. Staude, S. Cardanobile, and S. Rotter, *PLoS Computational Biology* **7** (2011), 10.1371/journal.pcbi.1002059.
- [12] M. Helias, T. Tetzlaff, and M. Diesmann, *PLoS Computational Biology* **10** (2014), 10.1371/journal.pcbi.1003428, arXiv:1304.2149.
- [13] N. Brunel, *Neurocomputing* **32-33**, 307 (2000).
- [14] V. Pernice, B. Staude, S. Cardanobile, and S. Rotter, *Physical Review E - Statistical, Non-linear, and Soft Matter Physics* **85**, 1 (2012), arXiv:arXiv:1201.0288v2.
- [15] J. Trousdale, Y. Hu, E. Shea-Brown, and K. Josić, *PLoS Computational Biology* **8** (2012), 10.1371/journal.pcbi.1002408, arXiv:1110.4914.
- [16] N. Brunel and V. Hakim, *Neural Computation* **11**, 1621 (1999), arXiv:9904278 [cond-mat].
- [17] B. Lindner and L. Schimansky-Geier, *Physical Review Letters* **86**, 2934 (2001).
- [18] S. Ostojic, *Nature neuroscience* **17**, 594 (2014).
- [19] S. Jovanović, J. Hertz, and S. Rotter, *Phys. Rev. E* **91**, 042802 (2015).
- [20] T. Deniz and S. Rotter, , 1 (2016), arXiv:1604.03619.
- [21] M. N. Shadlen and W. T. Newsome, *The Journal of neuroscience : the official journal of the Society for Neuroscience* **18**, 3870 (1998).
- [22] D. R. Lyamzin, S. J. Barnes, R. Donato, J. A. Garcia-Lazaro, T. Keck, and N. A. Lesica, *Journal of Neuroscience* **35**, 8065 (2015).
- [23] R. Rosenbaum, F. Marpeau, J. Ma, A. Barua, and K. Josić, *Journal of Mathematical Biology* **65**, 1 (2012), arXiv:1011.0669.
- [24] M. Helias, M. Deger, M. Diesmann, and S. Rotter, *Frontiers in computational neuroscience* **3**, 29 (2010).
- [25] A. Abouzeid and B. Ermentrout, *Physical Review E - Statistical, Nonlinear, and Soft Matter Physics* **84** (2011), 10.1103/PhysRevE.84.061914, arXiv:arXiv:1101.1919v1.
- [26] T. Tchumatchenko, A. Malyshev, T. Geisel, M. Volgushev, and F. Wolf, *Physical Review Letters* **104**, 2 (2010), arXiv:0810.2901.

- [27] R. D. Vilela and B. Lindner, *Physical Review E - Statistical, Nonlinear, and Soft Matter Physics* **80**, 1 (2009), arXiv:0912.2336.
- [28] T. Schwalger, F. Droste, and B. Lindner, *Journal of Computational Neuroscience* **39**, 29 (2015).
- [29] S. O. Voronenko, Stannat W, and Linder B, *The Journal of Mathematical Neuroscience* **5**, 1 (2015).
- [30] M. Schultze-Kraft, M. Diesmann, S. Grün, and M. Helias, *PLoS Computational Biology* **9**, e1002904 (2013), arXiv:1207.7228.
- [31] A. Kuhn, A. Aertsen, and S. Rotter, *Neural Computation* **15**, 67 (2003).
- [32] M. J. E. Richardson and R. Swarbrick, *Phys. Rev. Lett.* **105**, 178102 (2010).
- [33] M. Abramowitz, *Handbook of Mathematical Functions, With Formulas, Graphs, and Mathematical Tables*, (Dover Publications, Incorporated, 1974).
- [34] M.-O. Gewaltig and M. Diesmann, *Scholarpedia* **2**, 1430 (2007).
- [35] W. Gerstner and W. M. Kistler, *Spiking neuron models : single neurons, populations, plasticity* (Cambridge University Press, Cambridge, New York, Melbourne, 2002) autre tirage : 2006, 2008 (4e).
- [36] A. Kuhn, A. Aertsen, and S. Rotter, *Integration The Vlsi Journal* **24**, 2345 (2004).
- [37] J. de la Rocha, B. Doiron, E. Shea-Brown, K. Josić, and A. Reyes, *Nature* **448**, 802 (2007).
- [38] K. Padmanabhan and N. N. Urban, *Nature Neuroscience* **13**, 1276 (2010).
- [39] M. Y. Yim, J. Wolfart, A. Aertsen, and S. Rotter, *Frontiers in Computational Neuroscience* **6** (2012), 10.3389/conf.fncom.2012.55.00030.
- [40] M. Y. Yim, A. Aertsen, and S. Rotter, *Physical Review E - Statistical, Nonlinear, and Soft Matter Physics* **87**, 1 (2013), arXiv:1208.5350.
- [41] A. Morrison, M. Diesmann, and W. Gerstner, *Biological Cybernetics* **98**, 459 (2008).
- [42] B. Babadi and L. F. Abbott, *PLoS Computational Biology* **9**, e1002906 (2013).
- [43] S. Ostojic, N. Brunel, and V. Hakim, *J Neurosci* **29**, 10234 (2009).
- [44] M. Y. Yim, A. Kumar, A. Aertsen, and S. Rotter, *Journal of Computational Neuroscience* , 293 (2014).
- [45] E. Shea-Brown, K. Josić, J. de la Rocha, and B. Doiron, *Physical Review Letters* **100**, 108102 (2008).
- [46] B. Staude, S. Rotter, and S. Grün, in *Analysis of Parallel Spike Trains*, edited by S. Rotter

and S. Grün (Springer, 2010) Chap. 12, pp. 253–283.

[47] W. F. Ames, *Numerical methods for partial differential equations* (Academic press, 2014).